

# Synthesis and Self-Assembly of Rod-Coil Molecules with n-Shaped Rod Building Block

KE-LI ZHONG,<sup>1</sup> ZHEGANG HUANG,<sup>2</sup> ZHIJIN MAN,<sup>1</sup> LONG YI JIN,<sup>1,3</sup> BINGZHU YIN,<sup>1</sup> MYONGSOO LEE<sup>2</sup>

<sup>1</sup>Key Laboratory for Organism Resources of the Changbai Mountain and Functional Molecules, Ministry of Education and Department of Chemistry, College of Science, Yanbian University, No. 977 Gongyuan Road, Yanji 133002, People's Republic of China

<sup>2</sup>Department of Chemistry, Seoul National University, Seoul 151-747, Korea

<sup>3</sup>School of Natural Sciences, University of California, Merced, California 95343

Received 1 December 2009; accepted 18 December 2009

DOI: 10.1002/pola.23909

Published online in Wiley InterScience (www.interscience.wiley.com).

**ABSTRACT:** The rod-coil molecules with n-shaped rod building block, consisting of an anthracene unit and two biphenyl groups linked together with acetylenyl bonds at the 1,8-position of anthracene as a rigid rod segment, and the alkyl or alkyloxy chains with various length (i.e., methoxy- (**1**), octyl- (**2**), hexadecyl- (**3**)) at the 10-position of anthracene and poly(ethylene oxide) with the number of repeating units of 7 connected with biphenyl as coil segments were synthesized. The molecular structures were characterized by <sup>1</sup>H NMR and MALDI-TOF mass spectroscopy. The self-assembling behavior of new type of molecules **1–3** was investigated by means of DSC, POM, and SAXS at the bulk state. These molecules with a n-shaped rod building block segment self-assemble into supramolecular structures through the com-

ination of  $\pi$ - $\pi$  stacking of rigid rod building blocks and microphase separation of the rod and coil blocks. SAXS studies reveal that molecules **1** and **2** show hexagonal columnar and rectangular columnar structures in the liquid crystalline phase, respectively; meanwhile, molecules **1–3** self-organize into lamellar structures in the crystalline state. In addition, self-assembling studies of molecules **1–3** by DLS and TEM indicated that these molecules self-assemble into elongated nanofibers in aqueous medium. © 2010 Wiley Periodicals, Inc. *J Polym Sci Part A: Polym Chem* 48: 1415–1422, 2010

**KEYWORDS:** n-shaped; rod-coil; SAXS; self-assembly; supramolecular structures

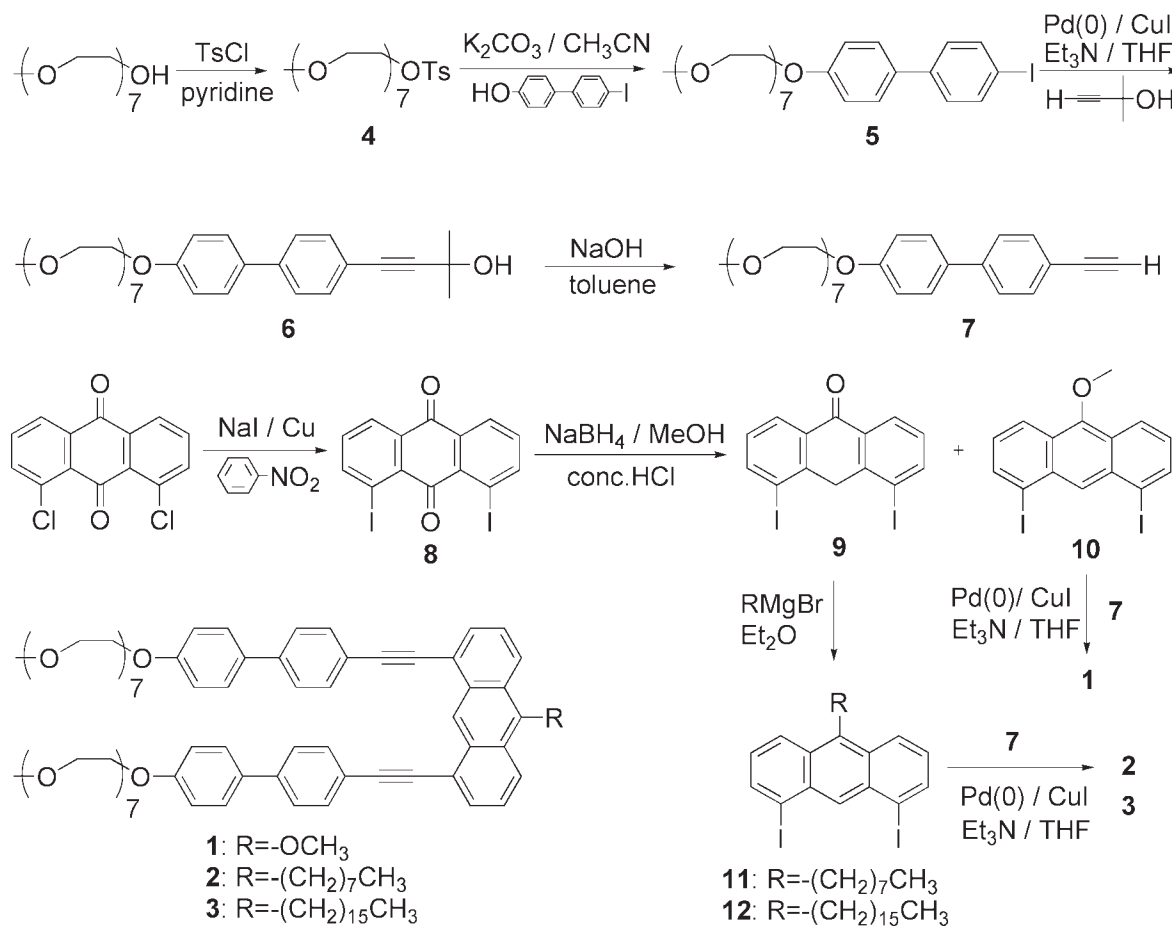
**INTRODUCTION** Self-assembly of conjugated molecular systems through noncovalent forces including hydrophobic and hydrophilic effects, electrostatic interaction, hydrogen bonding, and microphase segregation can be widely used because of their remarkable potentials as advanced functional materials in areas of biochemistry, molecular electronics, biomimetic chemistry, and materials science.<sup>1–5</sup> Among self-assembling molecular systems, conjugated rod-coil block molecules facile provide the spontaneous generation of a well-defined supramolecular architecture.<sup>6</sup> The supramolecular structures can be precisely controlled by systematic variation of the molecular shape and volume fraction of specific segments.<sup>7–9</sup> The self-assembling studies concerning supramolecular structures and the intriguing properties have been reported, focusing on various shapes of rigid conjugated rod segment, such as Y shaped,<sup>10–12</sup> T shaped,<sup>13,14</sup> O shaped,<sup>15</sup> K shaped,<sup>16</sup> propeller shaped,<sup>17</sup> and dumbbell like.<sup>18</sup> The results showed that incorporation of flexible coil segments into the conjugated rod building block lead to various shaped molecules

and these molecules self-organize into unique self-assembling or aggregation structures, such as 1D lamellar, 2D columnar, cylinders, discrete bundles, ribbons, and vesicles. One example is that we have systematically studied a dumbbell-shaped molecule that can self-assemble into a capsule structure with responsive gated nano-pores undergoing a transition from the open state to the closed state upon heating, which is capable of blocking cargo transport.<sup>18</sup> Hence, such a system has the potential to be developed as the gated plasma membrane of an artificial cell. In particular, there is growing interest in the design of synthetic rod-coil molecules with conjugated n-shaped rod building block that are able to self-assemble into supramolecular nanostructures for application in biochemistry and materials science.

With this in mind, for the first time, we synthesized rod-coil molecules **1–3** (see Scheme 1) with conjugated n-shaped rod building blocks and investigated their self-assembling behaviors in bulk state and an aqueous solution by using differential scanning calorimetry (DSC), thermal polarized optical

Additional Supporting Information may be found in the online version of this article. Correspondence to: L. Y. Jin (E-mail: lyjin@ybu.edu.cn) or M. Lee (E-mail: myongslee@snu.ac.kr)

*Journal of Polymer Science: Part A: Polymer Chemistry*, Vol. 48, 1415–1422 (2010) © 2010 Wiley Periodicals, Inc.


**SCHEME 1** Synthetic route of molecules 1–3.

microscopy (POM), small-angle X-ray scatterings (SAXS), and transmission electron microscopy (TEM).

## EXPERIMENTAL

### Materials

Poly(ethylene glycol) methyl ether ( $M_w = 350$ ), toluene-*p*-sulfonyl chloride (TsCl, 98%), 2-methyl-3-butyn-2-ol, cuprous iodide, sodium iodide, copper powder, 1-bromopentadecane, 1-bromooctane (all from Aldrich), tetrakis(triphenylphosphine) palladium(0), sodium borohydride, 4-hydroxy-4'-iodobiphenyl, 1,8-dichloro-anthraquinone (all from TCI), and the conventional reagents were used as received. Molecules **4** and **8–12** were prepared according to the procedures described elsewhere (see Supporting Information).<sup>19–21</sup>

### Measurements

<sup>1</sup>H NMR spectra were recorded from CDCl<sub>3</sub> solutions on a Bruker AM 300 spectrometer. A Perkin–Elmer Pyris Diamond differential scanning calorimeter was used to determine the thermal transitions, which were reported as the maxima and minima of their endothermic or exothermic peaks; the heating and cooling rates were controlled to 10 °C/min. X-ray scattering measurements were performed in transmission mode with synchrotron radiation at the 3C2 X-ray beam line at Pohang Accelerator Laboratory, Korea. A Nikon Optiphot

2-pol optical polarized microscope, equipped with a Mettler FP82 hot-stage and a Mettler FP90 central processor, was used to observe the thermal transitions and to analyze the anisotropic texture. Matrix-assisted laser desorption ionization time-of-flight mass spectroscopy (MALDI-TOF-MS) was performed on a perceptice Biosystems Voyager-DE STR using a 2-cyano-3-(4-hydroxyphenyl) acrylic acid (CHCA) as matrix. The UV-vis and the fluorescence spectra were obtained from a Shimadzu UV-1650PC spectrometer and a Hitachi F-4500 fluorescence spectrometer, respectively. Dynamic light scattering (DLS) measurements were performed by using a UNIPHASE He-Ne laser operating at 632.8 nm. The transmission electron microscope (TEM) was performed at 120 kV using JEOL 1020. Sample was stained by depositing a drop of 2 wt % uranyl acetate aqueous solution onto the surface of the sample-loaded grid and dried at 45 °C.

### Synthesis of Compound 5

Excess K<sub>2</sub>CO<sub>3</sub>, 4-hydroxy-4'-iodobiphenyl (3.0 g, 10 mmol), and compound **4** (5.5 g, 11 mmol) were dissolved in absolute acetonitrile (120 mL). The mixture was further refluxed for 12 h. The solvent was removed in a rotary evaporator and washed by water, and then the mixture was extracted with ethyl acetate and dried over anhydrous magnesium sulfate and filtered. After the solvent was removed in a rotary

evaporator, the crude product was purified by silica gel chromatography (EA as eluent) to yield 5.3 g of a yellow ropy liquid (85%).

$^1\text{H}$  NMR (300 MHz,  $\text{CDCl}_3$ ,  $\delta$ , ppm) 7.73(d, 2Ar-H, *o* to phenyl-I,  $J = 11.3$  Hz), 7.47(d, 2Ar-H, *m* to phenyl- $\text{OCH}_2$ ,  $J = 8.6$  Hz), 7.29 (d, 2Ar-H, *m* to phenyl-I,  $J = 11.3$  Hz), 6.98 (d, 2Ar-H, *o* to phenyl- $\text{OCH}_2$ ,  $J = 8.6$  Hz), 4.17 (t, 2H, phenyl $\text{OCH}_2\text{CH}_2\text{O}$ ,  $J = 4.8$  Hz), 3.88(t, 2H, phenyl $\text{OCH}_2\text{CH}_2\text{O}$ ,  $J = 4.8$  Hz), 3.54–3.74(m, 24H,  $-\text{OCH}_2\text{CH}_2\text{O}-$ ), 3.38(s, 3H,  $\text{OCH}_3$ ).

### Synthesis of Compound 6

Compound **5** (3.09 g, 5 mmol), 2-methyl-3-butyn-2-ol (1.26 g, 15 mmol),  $\text{Et}_3\text{N}$  (20 mL), CuI (15 mg, 0.08 mmol), and  $\text{Pd}(\text{PPh}_3)_4$  (50 mg, 0.04 mmol) were dissolved in THF (30 mL). The mixture was refluxed for 12 h under Ar, and then the solution was concentrated and washed by water. The mixture was extracted with ethyl acetate and dried over anhydrous magnesium sulfate and filtered. After the solvent was removed in a rotary evaporator, the crude product was purified by silica gel chromatography ( $\text{CH}_2\text{Cl}_2/\text{CH}_3\text{OH} = 20/1$  as eluent) to yield 1.72 g of a yellow ropy liquid (62%).

$^1\text{H}$  NMR (300 MHz,  $\text{CDCl}_3$ ,  $\delta$ , ppm) 7.42–7.52(m, 6Ar-H, *m* to  $\text{OCH}_2$ phenyl, *m* to phenyl-CC, *o* to phenyl-CC), 6.97(d, 2Ar-H, *o* to  $\text{CH}_2\text{O}$ phenyl), 4.17(t, 2H, phenyl  $\text{OCH}_2\text{CH}_2\text{O}$ ), 3.87(t, 2H, phenyl $\text{OCH}_2\text{CH}_2\text{O}$ ), 3.54–3.74(m, 24H,  $-\text{OCH}_2\text{CH}_2\text{O}-$ ), 3.37(s, 3H,  $\text{OCH}_3$ ), 1.63(s, 6H,  $\text{CH}_3$ ).

### Synthesis of Compound 7

Compound **6** (1.7 g, 3.0 mmol) and NaOH (1.2 g, 30 mmol) were dissolved in toluene (50 mL). The mixture was refluxed for 10 h, and then the solvent was removed and washed by water. The mixture was extracted with ethyl acetate and dried over anhydrous magnesium sulfate and filtered. After the solvent was removed in a rotary evaporator, the crude product was purified by chromatography on silica gel (EA: $\text{CH}_3\text{OH} = 5:1$  as eluent) to yield 1.1 g of a yellow liquid (70%).

$^1\text{H}$  NMR (300 MHz,  $\text{CDCl}_3$ ,  $\delta$ , ppm) 7.45–7.49(m, 6Ar-H, *m* to  $\text{OCH}_2$ phenyl, *m* to phenyl-CC, *o* to phenyl-CC), 6.94(d, 2Ar-H, *o* to  $\text{CH}_2\text{O}$ phenyl), 4.13(t, 2H, phenyl $\text{OCH}_2\text{CH}_2\text{O}$ ), 3.86(t, 2H, phenyl $\text{OCH}_2\text{CH}_2\text{O}$ ), 3.50–3.70(m, 24H,  $-\text{OCH}_2\text{CH}_2\text{O}-$ ), 3.34(s, 3H,  $\text{OCH}_3$ ), 3.11(s, 1H, CC–H).

### Synthesis of Molecules 1–3

Molecules **1–3** were synthesized by the same procedure. A representative example is described for **3**. Compound **12** (0.14 g, 0.21 mmol), Compound **7** (0.15 g, 0.5 mmol), CuI (15 mg, 0.08 mmol), and  $\text{Pd}(\text{PPh}_3)_4$  (50 mg, 0.04 mmol) were dissolved in THF (40 mL) and  $\text{Et}_3\text{N}$  (20 mL). The mixture was refluxed for 30 h under Ar, then was concentrated by evaporation and washed by water. The mixture was extracted with ethyl acetate and dried over anhydrous magnesium sulfate and filtered. After the solvent was removed in a rotary evaporator, the crude product was purified by silica gel chromatography (EA/ $\text{CH}_3\text{OH} = 4/1$  as eluent). The product was further purified by recycle gel permeation chromatography (JAI) to yield 100 mg of a yellow solid (48%).

$^1\text{H}$  NMR (300 MHz,  $\text{CDCl}_3$ ,  $\delta$ , ppm) 9.62(s, 1H, 9-anthracene-H), 8.24(d, 2H, 4,5-anthracene-H), 7.76(d, 2H, 2,7-anthracene-H), 7.49(m, 6H, 3,6-anthracene-H and *o* to phenyl-CC), 7.33(d, 8Ar-H, *m* to phenyl-CC), 6.84(d, 4Ar-H, *o* to  $\text{CH}_2\text{O}$ phenyl), 4.10(t, 4H, phenyl $\text{OCH}_2\text{CH}_2\text{O}$ ), 3.82(t, 4H, phenyl $\text{OCH}_2\text{CH}_2\text{O}$ ), 3.51–3.70(m, 50H,  $-\text{OCH}_2\text{CH}_2\text{O}-$  and anthracene- $\text{CH}_2$ ), 3.34(s, 6H,  $\text{OCH}_3$ ), 1.78(m, 2H, anthracene- $\text{CH}_2\text{CH}_2$ ), 1.55(m, 2H, anthracene- $\text{CH}_2\text{CH}_2\text{CH}_2$ ), 1.22–1.30(m, 24H,  $-\text{CH}_2\text{CH}_2-\text{CH}_3$ ), 0.86 (t, 3H,  $\text{CH}_3$ ). MALDI-TOF-MS  $m/z$  ( $\text{M}$ ) $^+$  1434, ( $\text{M}+\text{Na}$ ) $^+$  1457.

### Molecule 2

Yield: 52%;  $^1\text{H}$  NMR (300 MHz,  $\text{CDCl}_3$ ,  $\delta$ , ppm) 9.66(s, 1H, 9-anthracene-H), 8.28(d, 2H, 4,5-anthracene-H), 7.82(d, 2H, 2,7-anthracene-H), 7.54(m, 6H, 3,6-anthracene-H and *o* to phenyl-CC), 7.35(d, 8Ar-H, *m* to phenyl-CC), 6.84(d, 4Ar-H, *o* to  $\text{CH}_2\text{O}$ phenyl), 4.14(t, 4H, phenyl $\text{OCH}_2\text{CH}_2\text{O}$ ), 3.88(t, 4H, phenyl $\text{OCH}_2\text{CH}_2\text{O}$ ), 3.51–3.70(m, 50H,  $-\text{OCH}_2\text{CH}_2\text{O}-$  and anthracene- $\text{CH}_2$ ), 3.36(s, 6H,  $\text{OCH}_3$ ), 1.80(m, 2H, anthracene- $\text{CH}_2\text{CH}_2$ ), 1.59(m, 2H, anthracene- $\text{CH}_2\text{CH}_2\text{CH}_2$ ), 1.20–1.30(m, 24H,  $-\text{CH}_2\text{CH}_2-\text{CH}_3$ ), 0.87(t, 3H,  $\text{CH}_3$ ). MALDI-TOF-MS  $m/z$  ( $\text{M}$ ) $^+$  1319, ( $\text{M}+\text{Na}$ ) $^+$  1342.

### Molecule 1

Yield: 58%;  $^1\text{H}$  NMR (300 MHz,  $\text{CDCl}_3$ ,  $\delta$ , ppm) 9.50(s, 1H, 9-anthracene-H), 8.32(d, 2H, 4,5-anthracene-H), 7.80(d, 2H, 2,7-anthracene-H), 7.52(m, 6H, 3,6-anthracene-H and *o* to phenyl-CC), 7.38(d, 8Ar-H, *m* to phenyl-CC), 6.84(d, 4Ar-H, *o* to  $\text{CH}_2\text{O}$ phenyl), 4.17(m, 7H, anthracene- $\text{OCH}_3$  and phenyl- $\text{OCH}_2\text{CH}_2\text{O}$ ), 3.87(t, 4H, phenyl $\text{OCH}_2\text{CH}_2\text{O}$ ), 3.53–3.74(m, 48H,  $-\text{OCH}_2\text{CH}_2\text{O}-$ ), 3.36(s, 6H,  $\text{OCH}_3$ ). MALDI-TOF-MS  $m/z$  ( $\text{M}$ ) $^+$  1236, ( $\text{M}+\text{Na}$ ) $^+$  1259.

## RESULTS AND DISCUSSION

### Synthesis of Molecules 1–3

The synthetic route of the rod-coil molecules with a n-shaped rod building block, consisting of an anthracene unit and two biphenyl groups linked together with acetylenyl bonds at the 1,8-position of anthracene as a rigid rod segment, and the alkyl or alkyloxy chains with various length (methoxy- (**1**), octanyl- (**2**), hexadecyl- (**3**)) at the 10-position of anthracene and poly(ethylene oxide) with the number of repeating units of 7 connected with biphenyl as coil segments was outlined in Scheme 1. Compound **7** was obtained from successive reactions of tosylation, nucleophilic substitution, sonogashira coupling, and demethylation using poly(ethylene glycol) methyl ether ( $M_w = 350$ ), 4-hydroxy-4'-iodobiphenyl and 2-methyl-3-butyn-2-ol as starting materials. 4,5-Diiodo-9-anthrone (**9**), 1,8-diiodo-10-methoxyanthracene (**10**), 1,8-diiodo-10-octylanthracene (**11**), and 1,8-diiodo-10-hexadecylanthracene (**12**) were synthesized according to the literature reported elsewhere.<sup>19,20</sup> Sonogashira coupling reaction of compound **7** with compound **10**, **11**, **12** successfully afforded rod-coil molecules **1**, **2**, **3** with n-shaped rod segment, respectively. The resulting block molecules were purified by silica gel column chromatography and then further purified by recycling preparative high performance liquid chromatography. The structure of molecules **1–3** were characterized by  $^1\text{H}$  NMR and MALDI-TOF mass

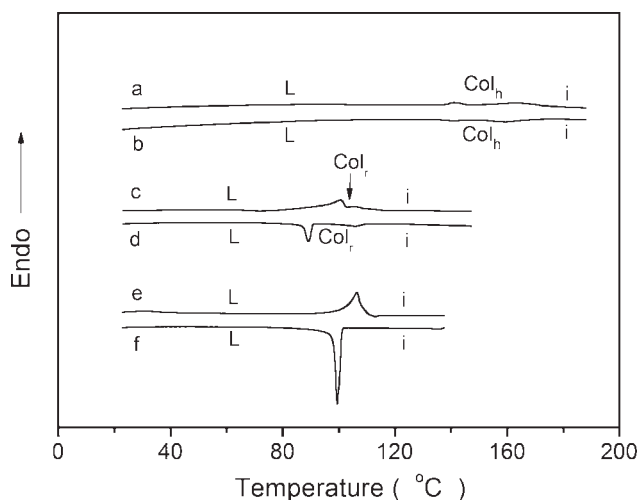


**FIGURE 1** DSC traces (10 °C/min) recorded during the second heating scan (a), the first cooling scan (b) of **1**; the second heating scan (c), the first cooling scan (d) of **2**; and the second heating scan (e) and the first cooling scan (f) of **3**.

spectroscopy (see Supporting Information Figures S1, S2) and were shown to be in full agreement with the structure presented in Scheme 1.

#### Structures of Bulk State

The self-assembling behavior of molecules **1–3** was investigated by DSC, thermal POM, and SAXS, Figure 2 shows the DSC heating and cooling traces and thermal transitions of the molecules **1–3**. Molecule **1**, connected with a methoxy group at 10 position of anthracene, shows an ordered bulk-state organization with bright birefringence, which transforms into an isotropic liquid at 163.2 °C [Fig. 1(a) and Table 1]. On slow cooling of **1**, from the isotropic liquid to liquid crystalline mesophase, the focal conical spherulitic fan texture was observed by POM experiment [Fig. 2(a)]. The DSC

**TABLE 1** Thermal Transitions of n-shaped Molecules (Data Are from Heating and Cooling Scans)

Molecule	$f_{\text{coil}}$	Phase Transition (°C)	
		Heating	Cooling
1	0.57	L 142.5 Col <sub>h</sub> 163.2 i	i 160.5 Col <sub>h</sub> 141 L
2	0.60	L 100.1 Col <sub>r</sub> 106.4 i	i 105.3 Col <sub>r</sub> 89.2 L
3	0.63	L 106.5 i	i 99.4 L

L, lamellar phase; Col<sub>h</sub>, hexagonal columnar phase; Col<sub>r</sub>, rectangular columnar phase; i, isotropy;  $f_{\text{coil}}$ , coil volume fraction.

curves together with optical texture preliminarily confirmed the presence of an ordered columnar phase. To identify the detailed self-organizing structures, X-ray scattering studies were performed. Several peaks with the ratio of 1: $\sqrt{3}$ : $\sqrt{4}$ : $\sqrt{9}$  in the small-angle region shown in Figure 3(b) can be indexed as the 100, 110, 200, 300 reflections of a 2D hexagonal columnar structure (see supporting information). From the observed  $d$  spacing of the 100 reflection, the lattice parameter of 2D hexagonal columnar phase of **1** is calculated to be 4.64 nm. From the experimental values of the unit cell parameters ( $a$ ,  $b$ ,  $c$ , and  $\gamma$ ) and the density ( $\rho$ ), the average number of molecules per cross-sectional slice of the column can be calculated according to eq 1, where  $M$  is the molecular mass and  $N_A$  is Avogadro's number. According eq 1, the average number ( $n$ ) of molecules in each bundle of **1** is calculated to be  $\sim 4$ . On the basis of the data, the schematic representation of the hexagonal columnar structure of **1** can be illustrated as shown in Figure 4(b).

$$n = \frac{abc \sin \gamma}{M/\rho N_A} \quad (1)$$

In addition, the small-angle X-ray diffraction patterns of the crystalline phases of **1** display several sharp reflections

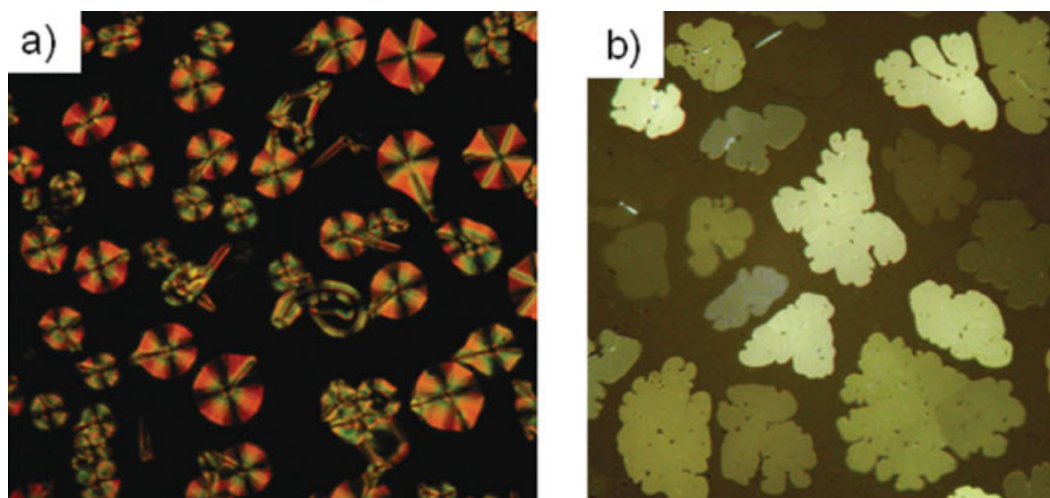


**FIGURE 2** Representative optical polarized micrograph ( $\times 100$ ) of the texture exhibited by (a) hexagonal columnar structure of **1** and (b) rectangular columnar structure of **2** at the transition from the isotropic liquid. [Color figure can be viewed in the online issue, which is available at [www.interscience.wiley.com](http://www.interscience.wiley.com).]

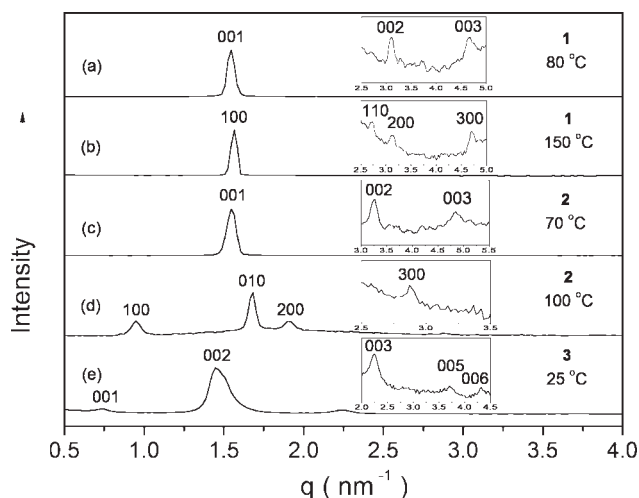


**FIGURE 3** Small-angle X-ray diffraction patterns of **1**, **2**, and **3** measured in solid state and melt state plotted against  $q$  ( $= 4\pi \sin \theta/\lambda$ ). (a) in the lamellar phase for **1** at 80 °C, (b) hexagonal columnar phase for **1** at 150 °C, (c) lamellar phase for **2** at 70 °C, (d) rectangular columnar phase for **2** at 100 °C, and (e) lamellar phase for **3** at 25 °C.

which correspond to equidistant  $q$ -spacings and thus index to a lamellar lattice. The layer spacing of 4.0 nm is very close to the corresponding estimated molecular length (4.5 nm by Corey-Pauling-Koltun (CPK) molecular model) indicative of a monomolecule layer structure in which rod segments are fully interdigitated [Figs. 3(a) and 4(a)].

Molecule **2**, incorporating an octyl group at 10 position of anthracene, also displays a columnar mesophase. Molecule **2** exhibits a birefringent liquid crystalline phase at a melting state (100.1 °C), followed by transformation to an isotropic

phase at 106.4 °C [Fig. 1(c) and Table 1]. Upon cooling from the isotropic liquid, a leaf-like texture with the characteristic of a columnar mesophase can be observed by using an optical polarized microscope [Fig. 2(b)]. The detailed liquid crystalline structure of **2** is also confirmed by small-angle X-ray scattering experiments. The small-angle X-ray scattering of **2** measured at cooling to 100 °C displays four sharp reflections that can be indexed as the 100, 010, 200, 300 that correspond to a two-dimensional rectangular columnar structure with lattice constants  $a = 6.6$  nm and  $b = 3.7$  nm [see Fig. 3(d) and Supporting Information]. This dimension implies that the more rod-like rigid segments arrange axially with their preferred direction within a cross-sectional slice of the column in which octyl chains pack in an interdigitated fashion. The average number of molecules in each supramolecular aggregate is calculated to be nearly 4 by eq 1 and the schematic representation of the rectangular columnar structure characterized by POM and SAXS can be illustrated as shown in Figure 4(d). Similar to molecule **1**, the structure of crystalline phase of molecule **2** also shows monomolecule layer with the interlayer spacing of 4.1 nm [Figs. 3(c) and 4(c)].

In sharp contrast to molecule **1**, molecule **3** contained a hexadecyl chain at 10 position of anthracene, only displays a 1D lamellar crystalline phase. There is only one endothermic and exothermic peak showed on DSC curves [Fig. 1(e,f)]. The small-angle X-ray diffraction patterns display several sharp reflections which correspond to equidistant  $q$ -spacings [Fig. 3(e)] and can be indexed to a lamellar lattice with the layer spacing of 8.6 nm. Considering the layer thickness obtained from the X-ray diffraction pattern is much larger than the estimated molecular length (6.2 nm by CPK model) and effect of the space filling requirement of n-shaped building block, bilayer arrangement of the rigid segments is expected

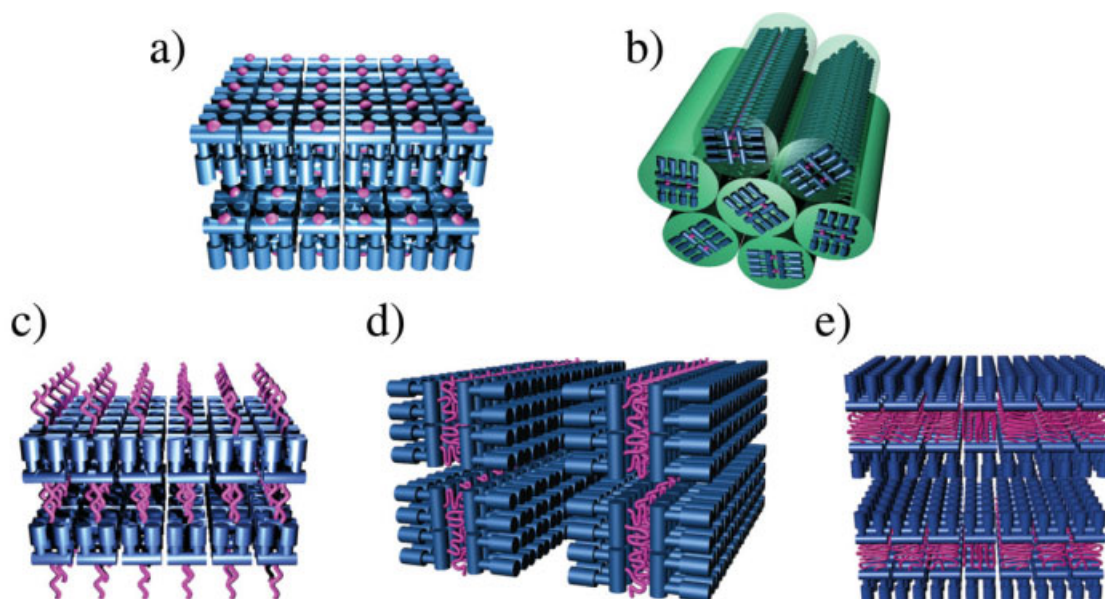


**FIGURE 4** Schematic representation of self-assembly of (a) monolayer structure for **1**, (b) hexagonal columnar structure for **1**, (c) monolayer structure for **2**, (d) rectangular columnar structure for **2**, and (e) bilayer structure for **3**.

**TABLE 2** Characterization of the Thermotropic Liquid Crystalline Behavior of Molecules 1–3 in Bulk State

Molecule	Crystalline Phase Lamellar <i>d</i> (nm)	Liquid Crystalline Phase					
		Hexagonal Columnar			Rectangular Columnar		
		<i>a</i> (nm)	<i>b</i> (nm)	<i>n</i>	<i>a</i> (nm)	<i>b</i> (nm)	<i>n</i>
1	4.0	4.64	4.64	4			
2	4.1				6.6	3.7	4
3	8.6						

*a*, *b*, the lattice constants; *n*, the average number of molecules per cross-sectional slice of the column; *d*, the layer spacing.

to be the best way to pack the hydrophobic segment, leading to a lamella structure [see Fig. 4(e)]. Furthermore, one interesting point is that the peak intensity associated with the (002) reflection appears to be the most intense, implying that distance of the rod segment within bilayer domain is 4.3 nm. On the basis of the DSC, POM, and XRD studies, char-

acterization of the self-assembling behavior of n-shaped molecules 1–3 in bulk state was summarized in Table 2.

### Aggregation Behavior in Aqueous Solution

Molecules 1–3 can be considered as a novel class of amphiphiles because it consists of hydrophilic flexible chain and hydrophobic rigid aromatic segment.<sup>22,23</sup> Aggregation behavior of molecules 1–3 was subsequently studied in aqueous solution using UV-vis and fluorescence spectra [Fig. 5(a)]. The absorption spectrum of 3 in aqueous solution (0.002 wt %) exhibits a broad transition with a maximum at 272 nm, resulting from the conjugated rod block. The fluorescence spectrum of 3 in chloroform solution (0.002 wt %) exhibits a strong emission maximum at 449 nm and 476 nm. However, the emission maximum in aqueous solution is blue-shifted with respect to that observed in chloroform solution, and the fluorescence is significantly quenched, indicative of aggregation of the conjugated rod segments [Fig. 5(a)].

DLS experiments of 3 were performed in aqueous solution to further investigate the aggregation behavior over a scattering angular range of 30°–130° [Fig. 5(b)]. The CONTIN

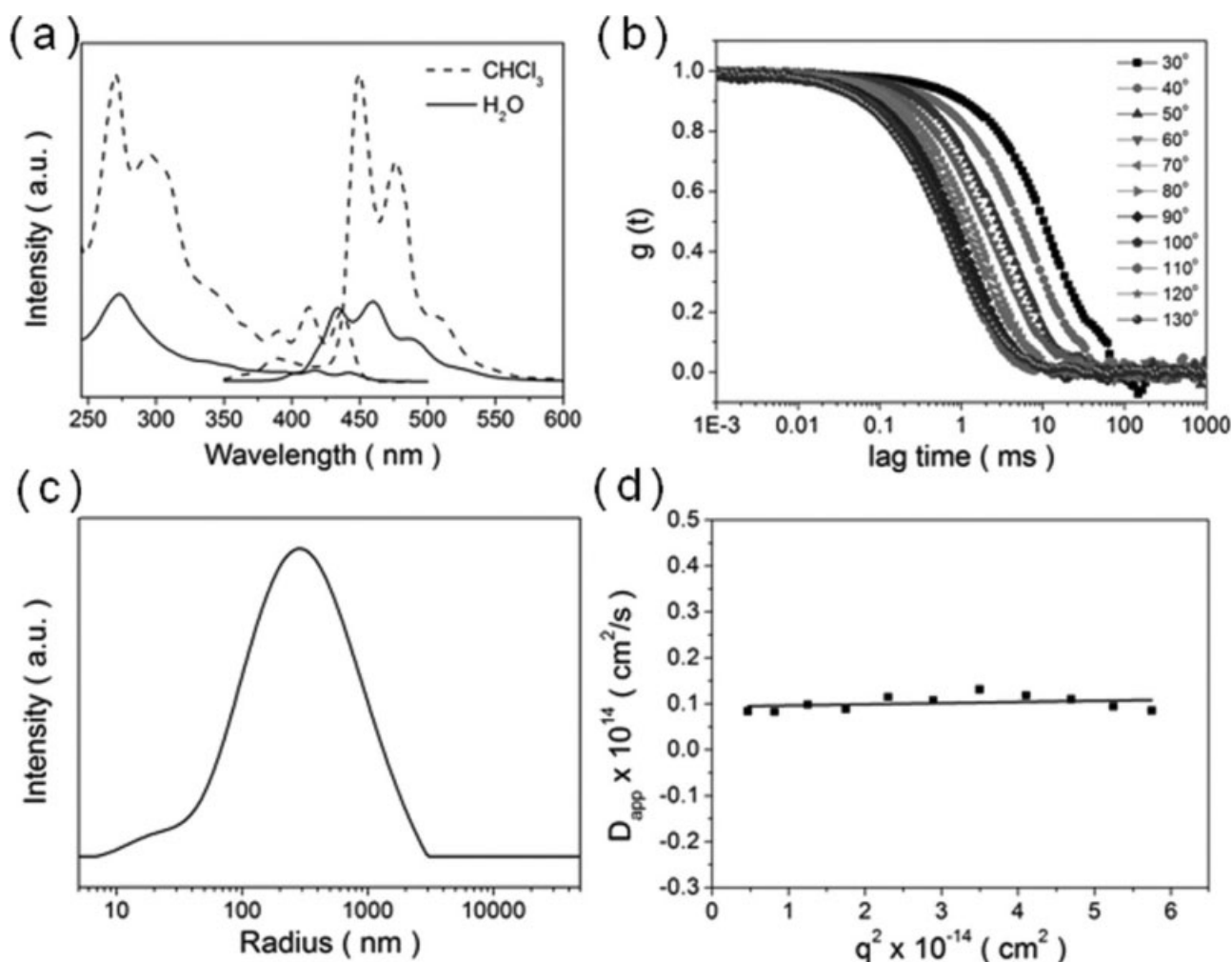


**FIGURE 5** (a) Absorption and emission spectra of 3 in  $\text{CHCl}_3$  and aqueous solution (0.002 wt %), (b) autocorrelation functions of 3 in aqueous solution (0.01 wt %), (c) hydrodynamic radius distribution of 3, and (d) angular dependence of diffusion coefficient for 3.



**FIGURE 6** TEM images (negatively stained with uranyl acetate) of sample cast from aqueous solution of (a) **1**, (b) **2**, and (c) **3** (scale bar = 100 nm).

analysis of the autocorrelation function at a scattering angle of  $90^\circ$  showed a broad peak corresponding to an average hydrodynamic radius (Rh) of  $\sim 295$  nm [Fig. 5(c)]. The angular dependence of the apparent diffusion coefficient was measured because the slope is related to the shape of the diffusing species. As shown in Figure 5(d), the slope value of 0.025 is consistent with the value predicted for elongated nonspherical micelles (0.03).<sup>24</sup> Molecules **1** and **2** showed similar aggregation behavior to that of **3** and their Rh value showed to be 112 nm and 260 nm, respectively.

To further confirm the aggregation structure, TEM experiments have been performed with an aqueous solution (Fig. 6). TEM micrograph of **3**, which obtained from a 0.01 wt % aqueous solution cast onto a TEM grid, clearly shows 1-dimensional nanofibers with a uniform diameter of 11.0 nm. Most of the strands have lengths up to several hundred nanometers. Considering the fully extended molecular length of the molecule **3** is estimated to be about 5.4 nm, the 11.0 nm width is consistent with sum of two molecular of **3**. Hence, the schematic representation of the nanofiber structure of **3** can be illustrated as shown in Figure 7. Remarkably, molecules **1** and **2** also self-assemble to elongated nanofibers with a uniform diameter of 7.0 nm and 9.0 nm, respectively, (Fig. 7).

On the basis of the results described above, the amphiphiles with a n-shaped aromatic segment can be considered to self-

assemble into elongated nanofibers with several micrometers length. The nanofibers consist of hydrophobic aromatic inner cores surrounded by hydrophilic flexible segments that are exposed to an aqueous environment. Within the core, the extended aromatic segments are stacked with a radial arrangement to release steric hindrance from bulky chains.

## CONCLUSIONS

Molecules **1–3** with a n-shaped rigid block segment, consisting of an anthracene unit, alkyl chain, and poly(ethylene oxide), were successfully synthesized and their self-assembling behavior in bulk and an aqueous solution was investigated. In the melt state, molecule **1** with a methoxy group at 10 position of anthracene self-assembles into a hexagonal columnar structure, Whereas molecule **2** with an octyl group at 10 position of anthracene self-organizes into rectangular columnar structure. Further increasing the length of alkyl chain suppresses a liquid crystalline phase and exhibits only a lamellar structure at solid state as in the case of **3**. The variation in the supramolecular structure can be explained by considering the microphase separation between the dissimilar parts of the molecule and the space-filling requirement of the flexible hydrophobic chains. Molecule **1** based on a methoxy group at the end of the rod segment can be packed with interdigitation of the rod segments, and

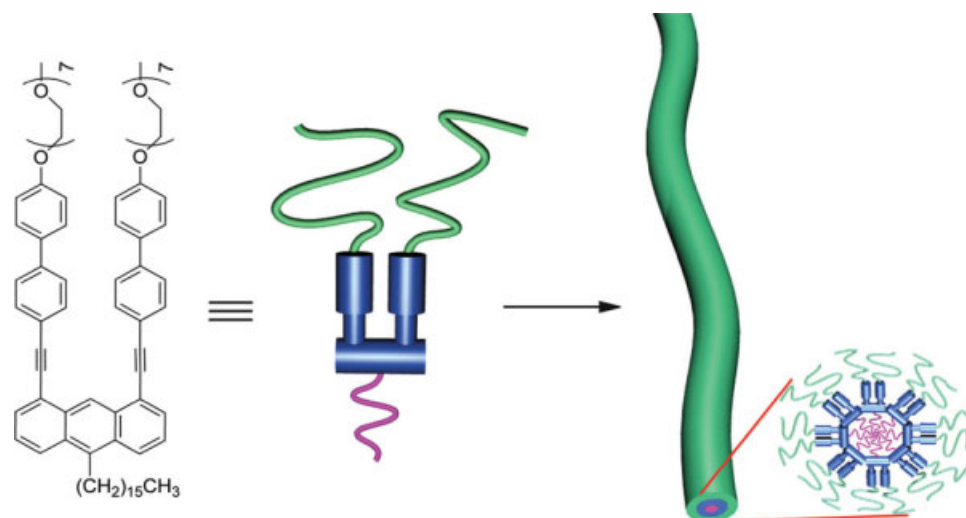


**FIGURE 7** Schematic representation of the proposed self-assembly of molecule **3** in aqueous solution. [Color figure can be viewed in the online issue, which is available at [www.interscience.wiley.com](http://www.interscience.wiley.com).]

increasing the length of the hydrophobic chain prohibits molecular interaction of the rod segments due to phase separation between aromatic rods and alkyl chains, resulting in the formation of 1D lamellar structure. In aqueous medium, molecules **1–3** can self-assemble into elongated nanofiber structure with a radial arrangement of the aromatic segments.

This work was supported by Program for New Century Excellent Talents in University, Ministry of Education, China, National Natural Science Foundation of China, and the National Creative Research Initiative Program of the Korean Ministry of Science and Technology.

## REFERENCES AND NOTES

- Vriezema, D. M.; Aragonés, M. C.; Elemans, J. A. A. W.; Cornelissen, J. J. L. M.; Rowan, A. E.; Nolte, R. J. M. *Chem Rev* 2005, 105, 1445–1490.
- Rudick, J. G.; Percec, V. *Acc Chem Res* 2008, 41, 1641–1652.
- Motoyanagi, J.; Fukushima, T.; Ishii, N.; Aida, T. *J Am Chem Soc* 2006, 128, 4220–4221.
- Hoeben, F. J. M.; Jonkhøj, P.; Meijer, E. W.; Schenning, A. P. H. J. *Chem Rev* 2005, 105, 1491–546.
- Rosen, B. M.; Wilson, C. J.; Wilson, D. A.; Peterca, M.; Imam, M. R.; Percec, V. *Chem Rev* 2009, 109, 6275–6540.
- Lee, M.; Cho, B. K.; Zin, W. C. *Chem Rev* 2001, 101, 3869–3892.
- Williams, D. R. M.; Fredrickson, G. H. *Macromolecules* 1992, 25, 3561–3568.
- Percec, V.; Mitchell, C. M.; Cho, W. D.; Uchida, S.; Glodde, M.; Ungar, G.; Zeng, X. B.; Liu, Y. S.; Balagurusamy, V. S. K.; Heiney, P. A. *J Am Chem Soc* 2004, 126, 6078–6094.
- Cho, B. K.; Lee, M.; Oh, N. K.; Zin, W. C. *J Am Chem Soc* 2001, 123, 9677–9678.
- Ryu, J. H.; Lee, E.; Lim, Y. B.; Lee, M. *J Am Chem Soc* 2007, 129, 4808–4814.
- Jang, C. J.; Ryu, J. H.; Lee, J. D.; Sohn, D.; Lee, M. *Chem Mater* 2004, 16, 4226–4231.
- Lee, E.; Kim, J. K.; Lee, M. *Angew Chem Int Ed* 2008, 47, 6375–6378.
- Moon, K. S.; Kim, H. J.; Lee, E.; Lee, M. *Angew Chem Int Ed* 2007, 46, 6807–6810.
- Liu, L. B.; Moon, K. S.; Gunawidjaja, R.; Lee, E.; Tsukruk, V. V.; Lee, M. *Langmuir* 2008, 24, 3930–3936.
- Ryu, J. H.; Oh, N. K.; Lee, M. *Chem Commun* 2005, 1770–1772.
- Lee, E.; Huang, Z.; Ryu, J. H.; Lee, M. *Chem Eur J* 2008, 14, 6957–6966.
- Moon, K. S.; Lee, E.; Lee, M. *Chem Commun* 2008, 3061–3063.
- Kim, J. K.; Lee, E.; Lim, Y. B.; Lee, M. *Angew Chem Int Ed* 2008, 47, 4662–4666.
- Goichi, M.; Segawa, K.; Suzuki, S.; Toyota, S. *Synthesis* 2005, 13, 2116–2118.
- Toyota, S.; Suzuki, S.; Goichi, M. *Chem Eur J* 2006, 12, 2482–2487.
- Zhong, K. L.; Chen, T.; Yin, B.; Jin, L. Y. *Macromol Res* 2009, 17, 280–283.
- Zhang, G.; Jin, W.; Fukushima, T.; Kosaka, A.; Ishii, N.; Aida, T. *J Am Chem Soc* 2007, 129, 719–722.
- Cuendias, A.; Ibarboure, E.; Lecommandoux, S.; Cloutet, E.; Henri Cramail, H. *J Polym Sci Part A: Polym Chem* 2008, 46, 4602–4616.
- Schmidt, M.; Stockmayer, W. H. *Macromolecules* 1984, 17, 509–514.